# BIBLIOGRAPHIC INFORMATION SYSTEM

**JOURNAL FULL TITLE:** Journal of Biomedical Research & Environmental Sciences
**ABBREVIATION (NLM):** J Biomed Res Environ Sci **ISSN:** 2766-2276 **WEBSITE:** https://www.jelsciences.com

## SCOPE & COVERAGE

- **Sections Covered:** 34 specialized sections spanning 143 topics across Medicine, Biology, Environmental Sciences, and General Science
- Ensures broad interdisciplinary visibility for high-impact research.

## PUBLICATION FEATURES

- **Review Process:** Double-blind peer review ensuring transparency and quality
- **Time to Publication:** Rapid 21-day review-to-publication cycle
- **Frequency:** Published monthly
- **Plagiarism Screening:** All submissions checked with iThenticate

## INDEXING & RECOGNITION

- **Indexed in:** Google Scholar, IndexCopernicus (**ICV 2022: 88.03**)
- **DOI:** Registered with CrossRef (**10.37871**) for long-term discoverability
- **Visibility:** Articles accessible worldwide across universities, research institutions, and libraries

## OPEN ACCESS POLICY

- Fully Open Access journal under Creative Commons Attribution 4.0 License (CC BY 4.0)
- Free, unrestricted access to all articles globally

## GLOBAL ENGAGEMENT

- **Research Reach:** Welcomes contributions worldwide
- **Managing Entity:** SciRes Literature LLC, USA
- **Language of Publication:** English

## SUBMISSION DETAILS

- Manuscripts in Word (.doc/.docx) format accepted

## SUBMISSION OPTIONS

- **Online:** https://www.jelsciences.com/submit-your-paper.php
- **Email:** support@jelsciences.com, support@jbresonline.com

HOME ABOUT ARCHIVE SUBMIT MANUSCRIPT APC

**Vision:** The Journal of Biomedical Research & Environmental Sciences (JBRES) is dedicated to advancing science and technology by providing a global platform for innovation, knowledge exchange, and collaboration. Our vision is to empower researchers and scientists worldwide, offering equal opportunities to share ideas, expand careers, and contribute to discoveries that shape a healthier, sustainable future for humanity.

JOURNAL OF BIOMEDICAL RESEARCH & ENVIRONMENTAL SCIENCES
ISSN: 2766-2276
SUBJECT AREA(S): NEPHROLOGY | PATHOLOGY
DOI: 10.37871

REVIEW ARTICLE

# FAM40A Deficiency Activates the Hippo Pathway to Promote Podocyte Apoptosis and Contribute to FSGS

**Chen Z and Guo Z***

The First Affiliated Hospital of Naval Medical University, Department of Nephrology, Shanghai, China

## Abstract

**Background:** Focal Segmental Glomerulosclerosis (FSGS), a major cause of end-stage renal disease, is characterized by podocyte loss via apoptosis and cytoskeletal disruption. Although dysregulation of the Hippo-YAP pathway is implicated in podocyte injury, upstream regulators of this pathway in FSGS pathogenesis remain elusive.

**Methods:** To determine whether FAM40A deficiency precipitates FSGS, we generated heterozygous FAM40A+/− mice by CRISPR/Cas9-mediated deletion of exons 3-8 (Δex3-8 allele). At specified time points, kidneys were collected for histological examination (PAS, TEM), immunofluorescence, and Western blotting to quantify podocyte apoptosis and Hippo pathway activation. Finally, FAM40A+/− mice were randomly assigned to receive treatment with the MST1/2 inhibitor XMU-MP-1 (1 mg/kg/day) via intraperitoneal injection or vehicle treatment for 10 days. Endpoints included urinary Albumin-to-Creatinine Ratio (ACR), renal histology, podocyte density, and podocyte apoptosis markers.

**Results:** We identified FAM40A as a novel negative regulator of the Hippo pathway in podocytes. FAM40A directly suppressed the kinase activity of Mst1/2, thereby preventing phosphorylation and inactivation of the downstream effector YAP. FAM40A deficiency triggered Mst1/2 activation, leading to YAP phosphorylation, nuclear exclusion, and transcriptional repression. This cascade resulted in podocyte apoptosis and exacerbated FSGS phenotypes *In vivo*.

**Conclusion:** Our study defines the FAM40A-Mst1/2-YAP axis as a critical signalling pathway governing podocyte survival. Loss of FAM40A activates Hippo signalling to promote podocyte apoptosis and FSGS progression. While short-term MST1/2 inhibition ameliorates disease features in mice, further evaluation of safety and feasibility is required. These findings highlight FAM40A as a potential therapeutic target for FSGS.

***Corresponding author(s)**

**Guo Z,** The First Affiliated Hospital of Naval Medical University, Department of Nephrology, Shanghai, China

**Email:** drguozhiyong@163.com

**DOI:** 10.37871/jbres2240

**Submitted:** 05 December 2025

**Accepted:** 15 December 2025

**Published:** 16 December 2025



OPEN ACCESS

**Keywords**

- Focal segmental glomerulosclerosis
- Mst1/2-Hippo-YAP
- FAM40A

VOLUME: 6 ISSUE: 12 - DECEMBER, 2025

Scan Me

**How to cite this article:** Chen Z, Guo Z. FAM40A Deficiency Activates the Hippo Pathway to Promote Podocyte Apoptosis and Contribute to FSGS. J Biomed Res Environ Sci. 2025 Dec 16; 6(12): 1911-1928. doi: 10.37871/jbres2240, Article ID: JBRES2240, Available at: https://www.jelsciences.com/articles/jbres2240.pdf

## Introduction

Focal Segmental Glomerulosclerosis (FSGS) is a clinically and pathologically heterogeneous glomerular disorder and a leading cause of End-Stage Renal Disease (ESRD). Its hallmark features include segmental glomerular sclerosis, podocyte injury and depletion, and Glomerular Basement Membrane (GBM) thickening [1,2]. Podocyte loss, primarily mediated by apoptosis and cytoskeletal disorganization, constitutes the central pathological event, ultimately compromising the glomerular filtration barrier and leading to proteinuria and progressive renal decline.

The etiology of FSGS is complex, encompassing primary (Idiopathic) forms and secondary causes (e.g., viral infections, toxins, metabolic disorders). Genetic factors also play a significant role. Advances in high-throughput sequencing have identified over 50 FSGS-associated genes, predominantly involved in regulating podocyte structure and function, including cytoskeletal proteins (e.g., ACTN4, CD2AP), slit diaphragm components (e.g., NPHS1, NPHS2), ion channels (e.g., TRPC6), and transcription factors (e.g., WT1) [3-5]. Nevertheless, approximately 60% of familial FSGS cases remain genetically undefined, highlighting substantial undiscovered genetic heterogeneity and pathogenic mechanisms. Identifying novel FSGS genes and elucidating their molecular pathophysiology is thus crucial for refining genetic diagnostics and developing targeted therapies.

Through whole-exome sequencing of Chinese familial FSGS pedigrees, we identified FAM40A (Family with Sequence Similarity 40 Member A) as a novel candidate gene, specifically detecting an unreported missense variant (p.M521T) segregating with disease [5]. Bioinformatic analysis indicates FAM40A encodes an 837-amino acid protein implicated in cortical actin dynamics and cell morphology [6,7]. Subsequent *In vitro* studies demonstrated that FAM40A silencing in podocytes disrupts normal morphology, causes foot process effacement, induces F-actin disorganization, and reduces Nephrin expression, suggesting a critical role in podocyte integrity.

FAM40A (also known as STRIP1) functions as a core scaffold component of the evolutionarily conserved STRIPAK (Striatin-Interacting Phosphatase and Kinase) complex. STRIPAK regulates diverse cellular processes (e.g., proliferation, apoptosis, polarity, migration) by modulating substrate phosphorylation/dephosphorylation and is implicated in major diseases, including cancer [8,9]. Crucially, FAM40A negatively regulates mammalian ste20-like kinases 1/2 (MST1/2) -- core upstream kinases of the Hippo pathway -- through direct binding to their phosphorylated forms in a phosphatase-dependent manner [8,10]. The Hippo pathway governs organ size, cell proliferation, apoptosis, morphology, and cytoskeletal reorganization by modulating the transcriptional co-activator YAP (Yes-associated protein). Pathway activation (*via* MST1/2 phosphorylation of LATS1/2 kinases) leads to YAP phosphorylation, cytoplasmic retention, and inactivation, promoting apoptosis [11-15]]. Conversely, pathway inactivation allows nuclear YAP translocation and pro-survival gene expression.

Mounting evidence implicates Hippo signaling dysregulation, particularly involving YAP, in FSGS pathogenesis. Seminal work demonstrated that podocyte-specific YAP deletion induces FSGS lesions and renal failure in mice, establishing YAP activity imbalance as a pivotal molecular event. Furthermore, Hippo pathway activation in podocytes is strongly linked to aberrant cytoskeletal remodelling [16]. However, the upstream mechanisms regulating YAP in podocytes, particularly the involvement of STRIPAK components like FAM40A, remain incompletely defined. We hypothesize that

FAM40A deficiency or dysfunction may activate MST1/2, leading to YAP phosphorylation/inhibition, subsequent podocyte apoptosis, and ultimately FSGS. This suggests the FAM40A-MST1/2-YAP axis represents a novel pathogenic mechanism.

# Methods

## Animals and genotyping

All animal experiments were approved by the Institutional Animal Care and Use Committee of Naval Medical University. Mice were housed under specific pathogen-free conditions with a 12-hour light/dark cycle and free access to food and water. The heterozygous FAM40AΔex3-8/+ mouse model (hereafter referred to as FAM40A+/-) was generated *via* CRISPR/Cas9-mediated deletion of exons 3–8 on a C57BL/6JCya background. Details of sgRNA design, embryo microinjection, founder identification, and breeding are described in sections 2.1–2.4. Genotyping was performed by PCR using tail DNA. Mice were identified as wild-type (WT, 454 bp band only), heterozygous (Het, 550 bp + 454 bp bands), or homozygous knockout (KO, 550 bp band only). Full germline FAM40A deletion was embryonic lethal, consistent with previous reports [17]; therefore, heterozygous mice were used for all subsequent studies.

## Experimental design and groups

For phenotypic characterization, male FAM40A+/- (Het) mice and their WT littermates ($n$ = 5 per group, all male) were analysed. Urine and serum samples were collected at specified time points (weeks 8-18). Mice were euthanized at week 13 or week 18 for histopathological and biochemical analyses. For the therapeutic intervention study, 13-week-old male FAM40A+/- mice ($n$ = 10) with established proteinuria and early FSGS pathology were used. Age-matched male WT littermates ($n$ = 5) served as normal controls. FAM40A+/- mice were completely randomized and assigned to two groups ($n$ = 5 each): (1) Vehicle group (Het + Vehicle): Received solvent *via* intraperitoneal (i.p.) injection. (2) XMU-MP-1 group (Het + XMU-MP-1): Received XMU-MP-1 (1 mg/kg/day, i.p.). The normal control group (WT + Vehicle) received solvent. Treatment lasted for 10 consecutive days. Group assignment and outcome assessments were performed by investigators blinded to the treatment allocation.

## CRISPR/Cas9 design and synthesis

A pair of single-guide RNAs (sgRNAs) targeting intronic sequences flanking exons 3-8 of Strip1 (FAM40A) were designed using CRISPOR (http://crispor.tefor.net/). High-scoring sgRNAs (gRNA-A1: 5′-TCCTCGGGACGTGACACTAAAGG-3′; gRNA-A2: 5′-GAAGCCTCACTCCGGCAGAGAGG-3′) were synthesized as 1.5 nmol RNAs (GenScript).

## RNP assembly and embryo microinjection

Ribonucleoprotein (RNP) complexes were prepared by incubating 50 pmol sgRNA with 20 pmol Cas9 nuclease (NEB, M0646M) in RNase-free water for 10 min at 25 ˚C. Female C57BL/6JCya mice (3-4 weeks old) were superovulated by sequential intraperitoneal injections of pregnant Mare Serum Gonadotropin (PMSG) and human Chorionic Gonadotropin (hCG) 46-48 hours apart. Females were mated with fertile C57BL/6JCya males immediately following hCG injection. Zygotes were collected from the oviducts of euthanized females with confirmed vaginal plugs the following morning. Zygotes were maintained in M16 medium at 37 ˚C under 5% CO until microinjection. Assembled RNP complexes were microinjected into the pronuclei of zygotes using standard techniques under an inverted microscope. Successful injection was confirmed by transient pronuclear swelling (~2-3x).

## Embryo transfer and genotyping

Injected zygotes were cultured in M16 medium for 0.5-1 hour before transfer. Injected zygotes

were bilaterally transferred into the oviducts of pseudo pregnant female mice (generated by mating with vasectomized males). Recipient females were anesthetized, and surgery was performed under aseptic conditions. Pups were toe-clipped at P7; genomic DNA was screened by PCR spanning exons 3-8. Founder mice harboring large deletions within the target locus were identified by PCR product size shift. Founders were backcrossed to wild-type C57BL/6JCya mice to establish the FAM40AΔex3-8/+ line; heterozygous intercrosses generated experimental cohorts.

## DNA extraction and PCR

Extract mouse tail DNA using the TaKaRa MiniBEST Universal Genomic DNA Extraction kit (Ver.5.0_Code No.9765) according to the manufacturer's instructions. One microliter of DNA supernatant served as template in a 25 μL reaction containing 1× Premix Taq Polymerase (Vazyme, P222) and 0.4 μM each primer. Two primer pairs were employed:

Set1 (550 bp amplicon specific for the deletion allele): Forward′-GACTGGCTGTTTTCCTACTTATTCCTAT-3′ and reverse 5′-AGAGCCAGTTCTTTCAAACGTCAG-3′.

Set2 (454 bp wild-type allele): forward 5′-GTGGTCTGTTTCCTGAGGATGTGT-3′ and reverse 5′-AGAGCCAGTTCTTTCAAACGTCAG-3′.

Thermal cycling: 94 ˚C for 3 min; 35 cycles of 94 ˚C for 30 s, 60 ˚C for 35 s, 72 ˚C for 35 s; final extension 72 ˚C for 5 min. Products were resolved on 2 % agarose gels and interpreted as follows: wild-type (454 bp only), heterozygous (550 + 454 bp).

## Clinical and histopathological assessment

Ten male mice (five FAM40A+/- and five Wild-Type (WT) littermates) were analysed. Urinary albumin and creatinine were quantified from 24-h metabolic-cage collections at weeks 8–12; the Albumin-to-Creatinine Ratio (ACR) was calculated. At week 13, serum creatinine was measured. Mice were then euthanized by cervical dislocation; kidneys were bisected. One part was fixed in 4 % paraformaldehyde (24 h) for PSA staining, immunohistochemistry, and immunofluorescence; the other part was immersed in electron-microscopy fixative for transmission electron microscopy.

## Urinary microalbumin measurement

Urinary microalbumin concentrations were quantified using a commercially available mouse-specific sandwich ELISA kit (Shanghai Enzyme Linked Biotechnology, Cat# ml037573) according to the manufacturer's instructions. Standards (50 μL/well) and urine samples (50 μL/well) were pipetted into standards wells and samples wells. Horseradish Peroxidase (HRP)-conjugated detection antibody (100 μL/well) was added to all wells except blanks. After sealing, the plate was incubated at 37°C for 60 minutes. After washing, 50 μL each of substrate solution A and B were added to all wells. The plate was incubated for 15 minutes in the dark. The reaction was stopped by adding 50 μL stop solution per well. Absorbance was measured at 450 nm within 15 minutes using a microplate reader. Sample concentrations were calculated from the standard curve generated using the kit-provided standards.

## Creatinine quantification

Serum creatinine was measured enzymatically on the automated chemistry analyzer (BIOBASE) using a creatinine enzymatic assay kit (BIOBASE, 70127). Leave whole blood samples at room temperature for 2 hours, then centrifuge at 3000 rpm at 2-8°C for 15 minutes. Take the supernatant for testing. Prepare reagents and set up the equipment according to the manufacturer's instructions. In the first step endogenous creatine/creatinine are eliminated; subsequently, creatinine is

hydrolysed to creatine, then to sarcosine, and finally to HO, which couples with 4-AA and EMSE to form a quinone chromophore (546 nm, 37 ˚C, 10 min). Results were calculated against a linear calibration curve.

## PAS staining

Paraffin sections were de-paraffinized in xylene and rehydrated through graded ethanol (100 %, 95 %, 85 %, 5 min each). Slides were oxidized with 1 % periodic acid (15 min), rinsed in distilled water, incubating in the dark for 30 minutes in Schiff reagent. (Baiqiandu, B1010), and washed under water. Nuclei were counter-stained with hematoxylin (Baiqiandu, B1001), differentiated in differentiation medium (Baiqiandu, B1004), blued in bluing solution (Baiqiandu, B1005), dehydrated through absolute ethanol, cleared in xylene, and mounted with neutral balsam. Images were captured using the light microscope (Nikon, Japan).

## Immunofluorescence (IF) staining

Paraffin sections were dewaxed, rehydrated, and subjected to EDTA-based antigen retrieval (pH 8.0). After quenching endogenous autofluorescence and blocking with 5% BSA (Baiqiandu, B0018), sections were incubated overnight at 4 ˚C with primary antibodies diluted in PBS. Following three PBS washes, species-matched Alexa Fluor-conjugated secondary antibodies were applied for 50 min at room temperature in the dark. Nuclei were counterstained with DAPI. Slides were mounted in anti-fade medium and examined using an fluorescence microscope (Nikon, Japan) (DAPI: ex 330–380 nm, em 420 nm; FITC: ex 465-495 nm, em 515-555 nm; Cy3: ex 510-560 nm, em 590 nm).

## Transmission Electron Microscopy (TEM) examination

Tissue (<1 $mm^3$) were fixed in glutaraldehyde (ASPEN, AS1063), rinsed in 0.1 M PBS (pH 7.4), post-fixed with 1% osmium tetroxide, and dehydrated through graded ethanol. Samples were infiltrated overnight in 1:1 acetone/Epon-812 (SPI, 90529-77-4), followed by pure Epon-812 and polymerised at 60 ˚C for 48 h. Use a slicer (Leica, Leica UC7) to cut ultra-thin slices of 60-80 nm. Double staining with saturated uranyl acetate solution and lead citrate and examined with the TEM (FEI, Tecnai G2 20 TWIN).

## Western blotting

Treat the harvested cells with RIPA buffer (Biosharp, BL504A) containing a mixture of protease (ROCHE, 04693159001) and phosphatase inhibitors (Servicebio, G2007-1ML and G2008-1ML) to lyse them. Following lysis, equal amounts of protein were quantified, loaded and separated by SDS-Polyacrylamide Gel Electrophoresis (SDS-PAGE), and subsequently transferred to a PVDF membrane (Millipore, IPVH00010). Seal the membrane with skimmed milk for one hour, then incubate it overnight at 4°C with a diluted primary antibody. Wash the sample with TBST, add diluted secondary antibody and incubate at room temperature, then wash again with TBST. Visualize the signal using ECL luminescent liquid (Meilunbio, MA0186). Develop the bands using a chemiluminescence apparatus (Peiqing, JS-1070P) and quantified using IPWIN60 software. The primary antibodies used were anti-FAM40A antibody (Zenbio, 672072), anti-p-MST1 antibody (Abmart, P42569-3S), anti-p-YAP antibody (Proteintech, 29018-1-AP), and anti-Cleaved Caspase-3 antibody (Cell Signaling Technology, 9661s). Subsequently, secondary antibody detection was performed using horseradish peroxidase-conjugated AffiniPure goat anti-mouse IgG (Beyotime, #A0216) or goat anti-rabbit IgG (Beyotime, #A0208).

## Quantitative method for foot process effacement

Under an electron microscope, select a specific region of the glomerulus to ensure that it contains the entire GBM. Determine a fixed 1

μm length of GBM as the unit of measurement. Count the number of clearly visible foot processes along the selected 1 μm length of GBM. Repeat the measurement across multiple glomeruli and multiple regions to obtain sufficient data points. Calculate the average number of foot processes per micrometer of GBM and compare between mice of different genotypes.

### Glomerulosclerosis and mesangial hypercellularity quantification

For each kidney, 100 glomeruli per PAS-stained section were evaluated in a blinded fashion. Glomerulosclerosis and mesangial hypercellularity were graded on identical four-tier semi-quantitative scales: 0, absent; 1, 1-10% involvement; 2, 11-25%; 3, 26-50 %; 4, > 50%.

### Pharmacological intervention with MST1/2 inhibitor

Thirteen-week-old FAM40A+/- mice (established FSGS model) were randomized to receive either XMU-MP-1 (1 mg/kg/day, $n$ = 5) or vehicle ($n$ = 5) by intraperitoneal injection for 10 consecutive days. XMU-MP-1 was freshly dissolved in Kolliphor HS 15 (40 %, w/v) plus 0.1 % citric acid (1:1) to a final concentration of 0.2 mg/mL. Injection dosage of drug solution was set to 100 μL/20g. Twenty-four-hour urine ACR and serum creatinine were determined on day 11, after which animals were euthanized for renal histopathology.

## Statistical Analysis

Data were analyzed using GraphPad-Prism-7.0 software (San Diego, CA). Data are presented as mean ± standard deviation (SD). Differences between two groups were analyzed using unpaired two-tailed Student's t-test with Welch's correction. A $p$-value < 0.05 was deemed statistically significant. The exact $p$-values and sample sizes ($n$) are provided in the figure legends.

## Results

### Generation and validation of the FAM40A-deficient mouse model

To test whether podocytes lacking FAM40A are intrinsically vulnerable to injury *In vivo*, we generated a mouse line carrying a heterozygous frameshift deletion of exons 3-8 of Strip1 (Encoding FAM40A), designated as FAM40AΔex3-8/+ (FAM40A+/-). Full germline deletion proved embryonically lethal, consistent with previous reports [14]; therefore, heterozygous animals were used to model partial loss-of-function. Founder mice were identified by tail-PCR spanning the targeted region, and heterozygous animals were established by back-crossing to WT mice. Immunofluorescence of 4 % PFA-perfused kidneys revealed near-complete loss of FAM40A within glomeruli of FAM40A+/- mice, whereas WT littermates exhibited robust, discrete FAM40A staining along the podocyte membrane (Figures 1A,B). Western blotting confirmed a 45-75 % reduction in renal FAM40A protein (Figures 1C,D). Collectively, these data establish FAM40A+/- mice as a valid, partial-loss model suitable for interrogating the role of FAM40A in podocyte integrity and glomerular disease.

### FAM40A haploinsufficiency precipitates albuminuria and progressive renal insufficiency

Systematic urine collections revealed that neither FAM40A+/- nor WT littermates exhibited measurable proteinuria before 10 weeks of age (Figure 1E). The first overt rise in albumin excretion occurred abruptly between weeks 11 and 12 in heterozygous mice, with urinary ACR climbing to 248.2 ± 35.99 μg mg$^{-1}$---a twelve-fold increase compared with age-matched WT controls (20.61 ± 3.42 μg mg$^{-1}$; $p$ < 0.001; $n$ = 5 per group) (Figure 1E). This sustained hyper-albuminuria coincided with a concomitant decline in renal function. Serum

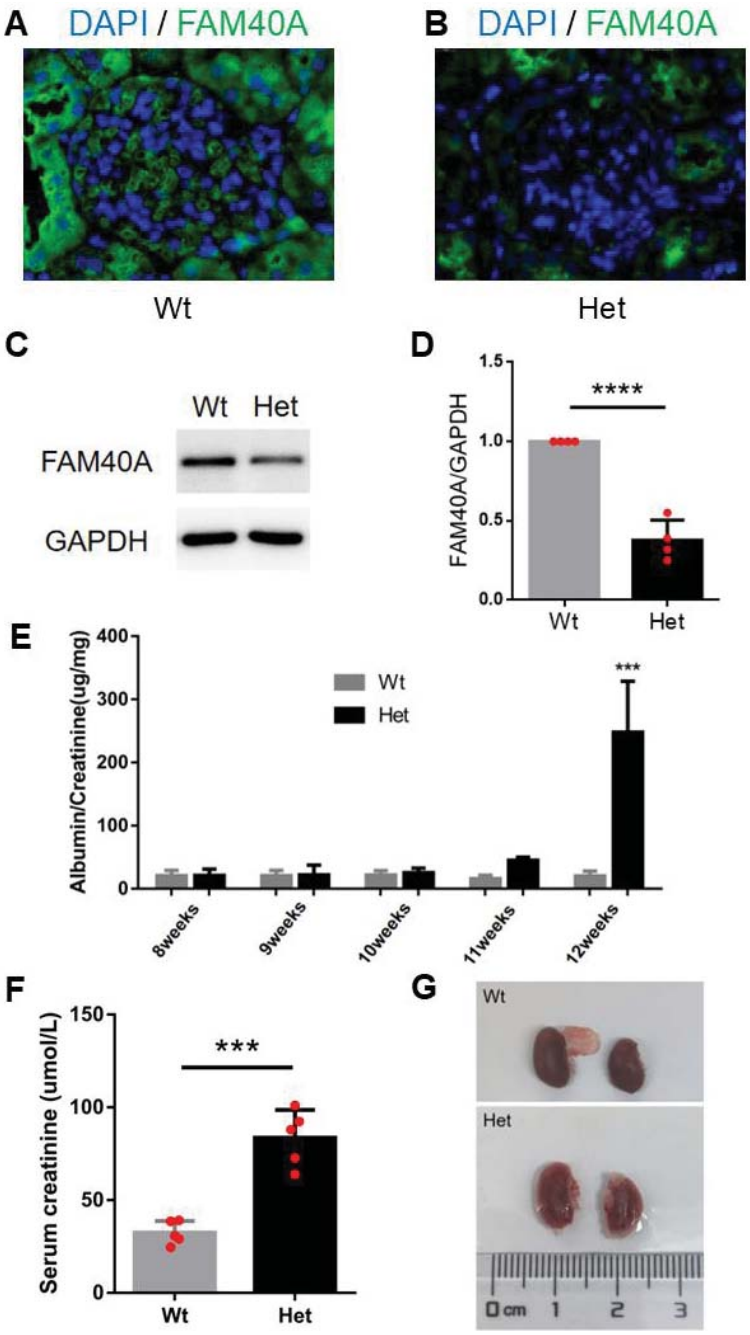


**Figure 1** FAM40A deficiency induces renal dysfunction and pathological changes in mice.
(A) Immunofluorescence microscopy shows that FAM40A (Green) is normally expressed in the glomeruli of WT mouse kidneys. Nuclei are stained with DAPI (Blue). Scale bar, 20 μm.
(B) FAM40A protein expression is reduced in the glomeruli of FAM40A+/− (Het) mice. Scale bar, 20 μm.(C, D) Western blot C) and quantification
(D) iIndicate partial silencing of FAM40A in kidney tissue of Het mice compared with WT control mice (Decrease of 45-75%). Data are mean ± SD; $n$ = 5 mice per group; ***$p$ < 0.001 by unpaired t-test.
(E) Urinary Albumin-to-Creatinine Ratio (ACR) demonstrating weekly progression of proteinuria in Het and WT mice. At week 12, $p$ < 0.001. Data are mean ± SD; $n$ = 5 per group.
(F) Serum creatinine measurements showing impaired kidney function in Het mice compared to WT controls at week 18. ***$p$ < 0.001. Data are mean ± SD; $n$ = 5 per group.
(G) Macroscopic appearance of kidneys from 13-week-old Het and WT mice. Het kidneys exhibit a corrugated capsule surface compared to the smooth surface of WT kidneys.

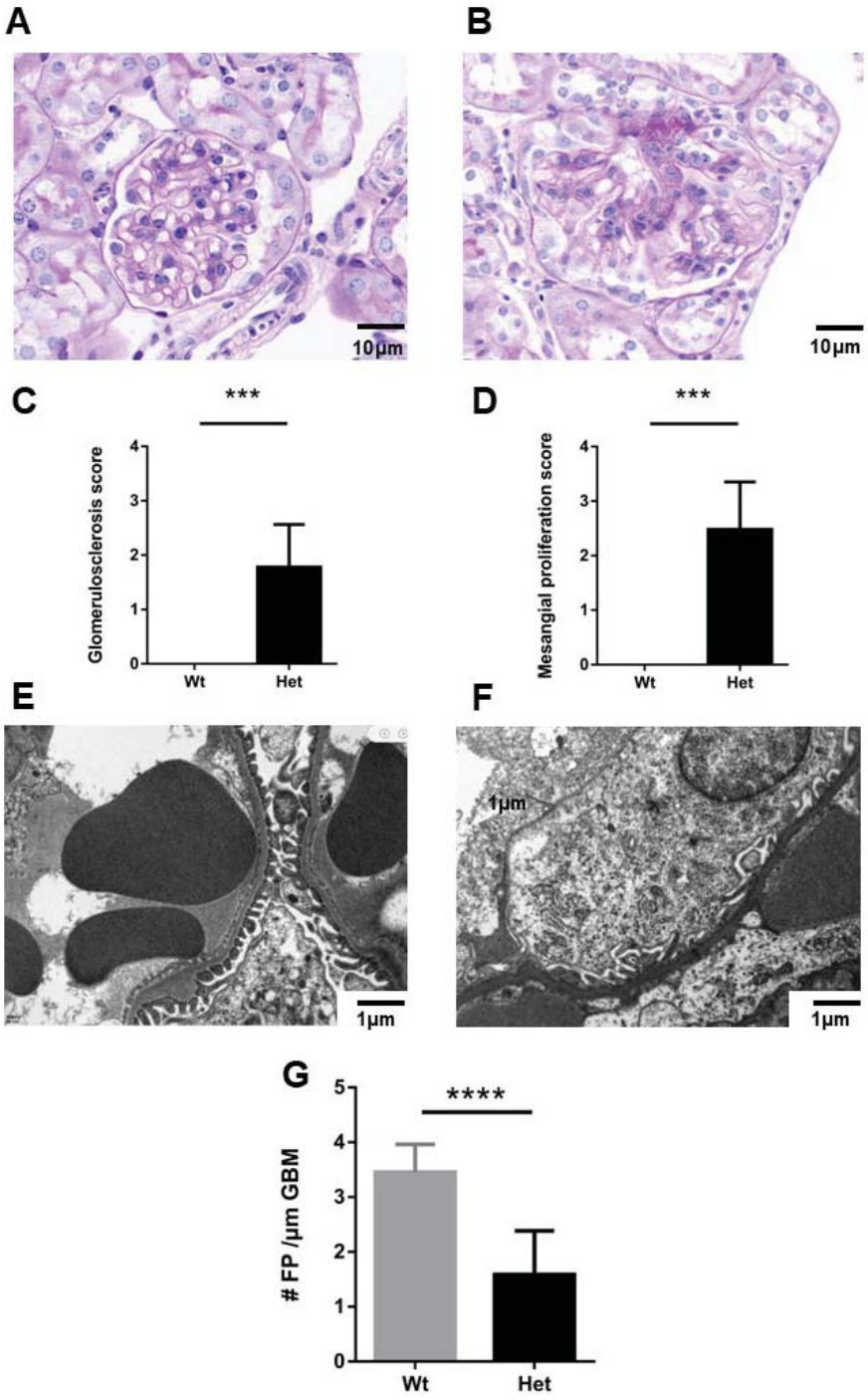


**Figure 2** FAM40A+/− heterozygous mice develop glomerular injury and podocyte foot process effacement.
(A) Representative PAS staining of a glomerulus from a WT mouse.
(B) Representative PAS staining of a glomerulus from a 13-week-old Het mouse showing focal segmental glomerulosclerosis (Arrow) and mesangial proliferation. Scale bars, 10 μm.
(C, D) Quantitative analysis of glomerulosclerosis score (C) and mesangial hypercellularity score (D) In 13-week-old mice. ***$p < 0.001$. Data are mean ± SD; $n = 5$ mice per group.
(E) Transmission Electron Microscopy (TEM) image of a glomerulus from a WT mouse showing intact foot processes (Arrows).
(F) TEM image of a glomerulus from a 13-week-old Het mouse showing diffuse foot process effacement (Arrowheads). Scale bars, 1 μm.
(G) Quantitative analysis of Foot Process (FP) density. Het: 1.59 ± 0.17 FP/μm; WT: 3.45 ± 0.11 FP/μm. ***$p < 0.001$. Data are mean ± SD; $n = 5$ mice per group.

creatinine---measured enzymatically at 18 weeks---was markedly elevated in FAM40A+/- animals (83.64 ± 6.73 µmol $L^{-1}$) relative to WT counterparts (32.51 ± 2.81 µmol $L^{-1}$; $p < 0.001$; $n$ = 5 per group; Figure 1F), signifying compromised glomerular filtration. Macroscopically, kidneys from 13-week-old FAM40A+/- mice displayed a finely granular, rippled capsular surface (Figure 1G), yet absolute kidney weight and organ size were indistinguishable between genotypes. Collectively, these data demonstrate that even partial loss of FAM40A is sufficient to initiate progressive proteinuria and culminate in overt renal dysfunction.

## The loss of FAM40A leads to FSGS

Serial renal histology revealed that FAM40A+/- mice remained histologically unremarkable at 8 weeks, yet developed progressive, proteinuria-associated lesions that peaked by week 13. PAS staining disclosed discrete foci of segmental glomerulosclerosis accompanied by marked mesangial expansion (Figures 2A,B); tubular architecture was preserved and interstitial inflammation was absent. Blind semiquantitative scoring confirmed significant increases in both glomerulosclerosis and mesangial hypercellularity versus wild-type littermates ($p < 0.001$; $n$ = 5 per group; Figures 2C,D).

Ultrastructural analysis corroborated these findings. Wild-type kidneys displayed orderly mesangial matrices and intact, regularly spaced foot processes (Figure 2E). By contrast, FAM40A+/- mice exhibited segmental foot-process effacement, slit-diaphragm disruption, irregular thickening of the GBM, and moderate mesangial matrix accumulation---hallmarks of FSGS (Figure 2F). Quantitative morphometry revealed a pronounced reduction in foot-process density (WT 3.45 ± 0.11 *vs.*, FAM40A+/- 1.59 ± 0.17-foot processes µm$^{-1}$ GBM; $p < 0.001$; $n$ = 5 per group) (Figure 2G). Collectively, these data establish that even partial loss of FAM40A is sufficient to drive the onset of FSGS *In vivo*.

FAM40A deficiency triggers podocyte apoptosis via hippo pathway activation

Given that FAM40A+/- heterozygous mice exhibit podocyte foot process effacement, we examined whether podocytes underwent apoptosis. Immunostaining of week-13 kidneys revealed abundant cleaved caspase-3 within glomeruli of FAM40A+/- mice, whereas littermate controls remained negative (Figure 3A). Western blotting corroborated this finding, demonstrating a marked increase in cleaved caspase-3 in mutant renal lysates (Figure 3B).

Concomitantly, we observed striking nuclear exclusion of YAP in mutant podocytes: phosphorylated YAP accumulated in the cytoplasm, contrasting with its predominant nuclear localization in wild-type cells (Figure 3C). Western blot analysis showed that compared with WT mice, the expression of Hippo pathway-related proteins was abnormal in the kidneys of FAM40A+/- heterozygous mice, specifically manifested as increased expression of phosphorylated MST1 (p-MST1) and phosphorylated YAP (p-YAP) ($p < 0.001$; n = 5 per group; Figures 3C,D). These findings suggest that podocyte apoptosis occurred in FAM40A+/- heterozygous mice, and the mechanism behind podocyte apoptosis is related to the overactivation of the Hippo pathway. XMU-MP-1 ameliorates proteinuria and pathological changes in FAM40A+/- mice

To evaluate the therapeutic potential of targeting the Hippo pathway, we treated 13-week-old FAM40A+/- mice (With established FSGS) with the MST1/2 inhibitor XMU-MP-1 or vehicle for 10 days. Compared with vehicle-treated control mice, XMU-MP-1-treated mice showed a significant decrease in urinary ACR (66.52 ± 8.185 µg/mg vs., 274.3 ± 33.62 µg/mg; $p < 0.001$; n = 5 per group; Figure 4A). There was no significant difference in serum creatinine levels between the two groups (36.51 ± 2.863

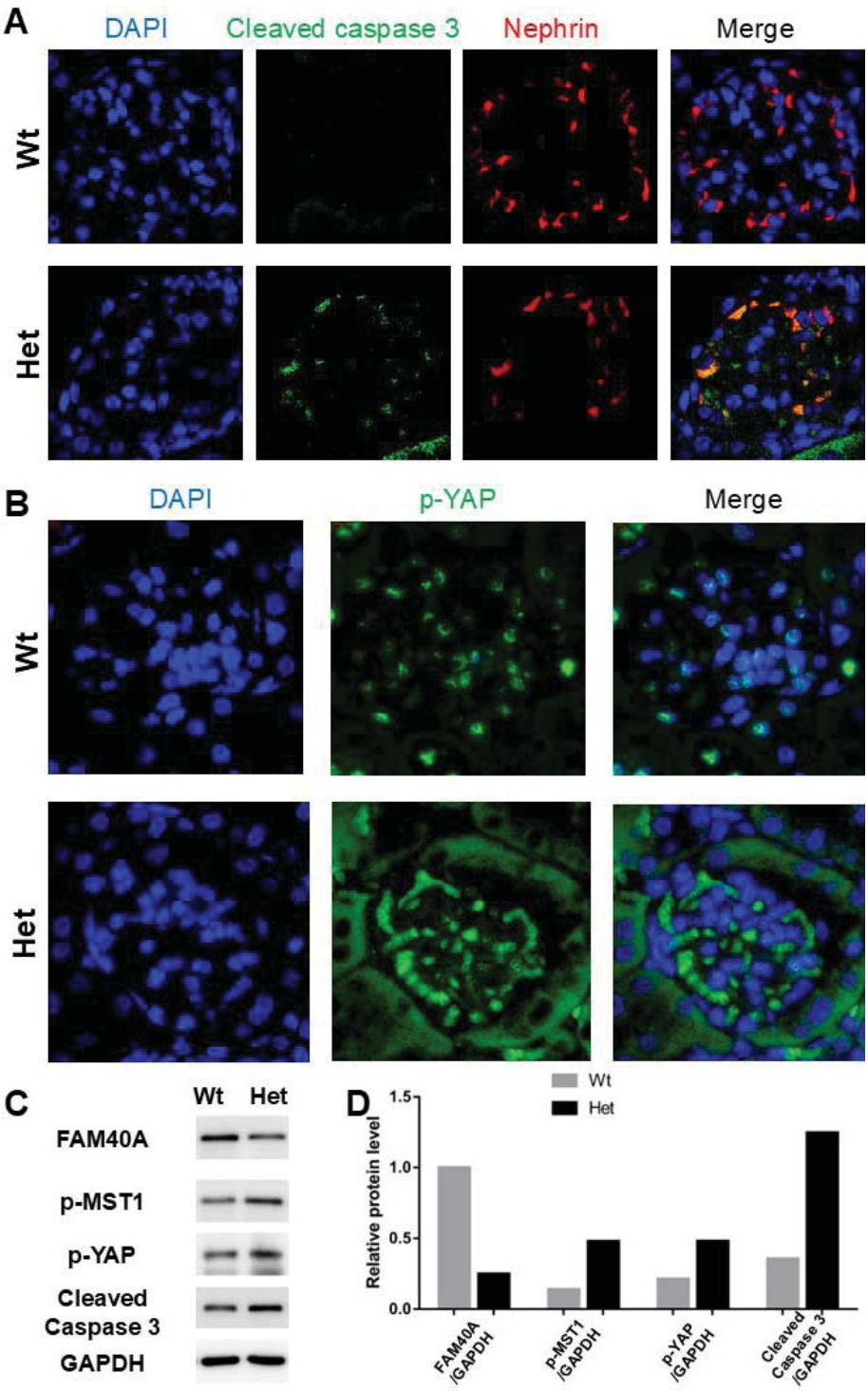


**Figure 3** FAM40A deficiency activates Hippo-mediated apoptosis in podocytes.
(A) Immunofluorescence staining for cleaved caspase-3 (Green, apoptosis marker) in kidney sections from 13-week-old WT and Het mice. Nuclei are stained with DAPI (Blue). Scale bars, 20 μm.
(B) Immunofluorescence staining for phosphorylated YAP (p-YAP, green) showing nuclear exclusion in Het podocytes compared to nuclear localization in WT. Nuclei are stained with DAPI (Blue). Scale bars, 20 μm.
(C) Representative Western blot examining protein expression of FAM40A, p-MST1, p-YAP, cleaved caspase-3, and GAPDH (Loading control) in kidney lysates from WT and Het mice at 13 weeks.
(D) Quantification of protein levels from (C), normalized to GAPDH. Data are mean ± SD; $n$ = 5 mice per group; *$p$ < 0.05, **$p$ < 0.01, ***$p$ < 0.001 vs., WT.

μmol/L vs., 39.94 ± 3.056 μmol/L; p = 0.4369; n = 5 per group; Figure 4B).

Electron microscopy results indicated that, compared with vehicle controls (Figure 4C), XMU-MP-1-treated mice exhibited reduced foot process effacement and a significant increase in foot process number (2.8 ± 0.12 vs., 1.5 ± 0.16 foot processes per micrometer; p < 0.001; n = 5 per group; Figures 4D,E). PAS staining showed that XMU-MP-1 intervention reduced segmental glomerulosclerosis and improved mesangial cell proliferation and matrix accumulation (Figures 5A,B). Semiquantitative scoring confirmed significant improvements in both glomerulosclerosis (1.07 ± 0.08 vs., 1.45 ± 0.09; p = 0.0021; n = 5 per group) and mesangial hypercellularity scores (1.88 ± 0.09 vs., 2.28 ± 0.11; p = 0.006; n = 5 per group; Figures 5C,D). These results suggest that short-term pharmacological inhibition of MST1/2 can improve renal morphology in FAM40A+/- mice.

## XMU-MP-1 reduces podocyte apoptosis in FAM40A+/− Mice by inhibiting hippo signalling

To investigate the mechanism underlying the therapeutic effect, we examined Hippo pathway activity and apoptosis markers after XMU-MP-1 treatment. Western blotting revealed that, compared with vehicle-treated FAM40A+/- mice, kidney tissue from XMU-MP-1-treated

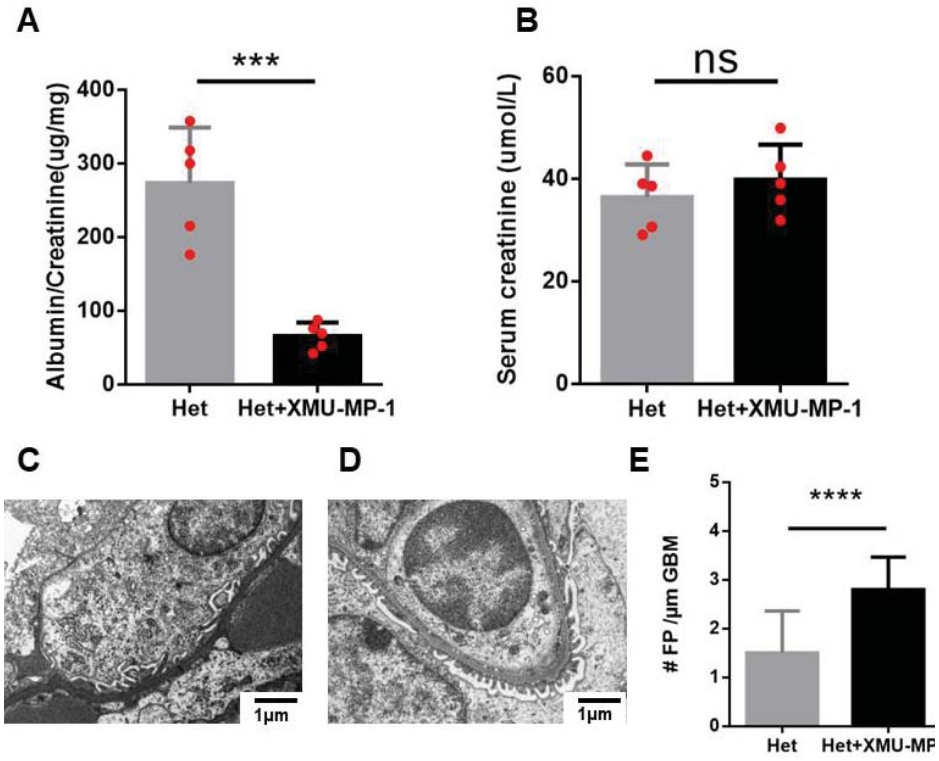


**Figure 4** Pharmacological inhibition of MST1/2 with XMU-MP-1 ameliorates renal injury in FAM40A+/− mice.
(A) Urinary ACR measurements in Het mice treated with vehicle (Het+Vehicle) or XMU-MP-1 (Het+XMU-MP-1) for 10 days. ***$p$ < 0.001. Data are mean ± SD; $n$ = 5 mice per group.
(B) Serum creatinine levels in the same groups. ns, not significant ($p$ = 0.4369). Data are mean ± SD; $n$ = 5 per group.
(C) Representative TEM image of a glomerulus from a vehicle-treated Het mouse showing foot process effacement.
(D) Representative TEM image of a glomerulus from an XMU-MP-1-treated Het mouse showing improved foot process architecture. Scale bars, 1 μm.
(E) Quantitative analysis of Foot Process (FP) density in Het mice with or without XMU-MP-1 treatment. ***$p$ < 0.001. Data are mean ± SD; $n$ = 5 mice per group.

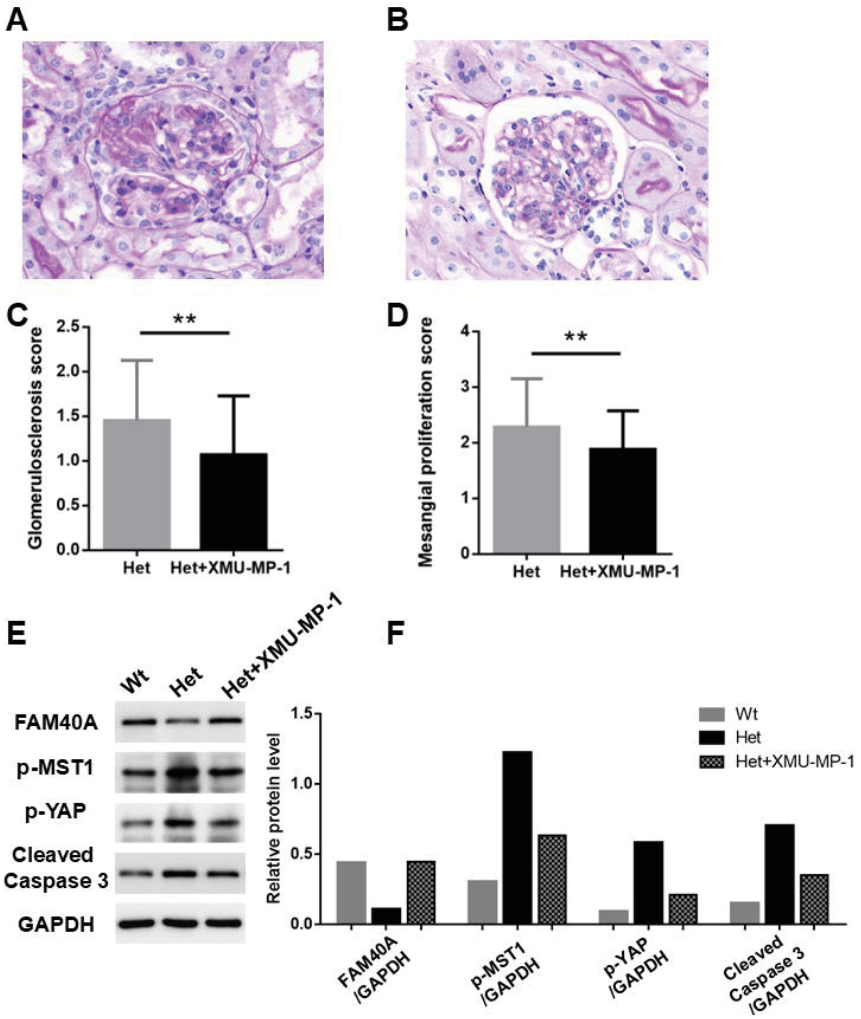


**Figure 5** Therapeutic targeting of MST1/2 attenuates glomerulosclerosis and podocyte apoptosis in FAM40A-deficient mice.
(A) Representative PAS staining of a glomerulus from a vehicle-treated het mouse showing segmental glomerulosclerosis (Arrow).
(B) Representative PAS staining of a glomerulus from an XMU-MP-1-treated Het mouse showing milder pathology. Scale bars, 10 μm.
(C) Quantitative analysis of glomerulosclerosis scores. $^{**}p = 0.0021$.
(D) Quantitative analysis of mesangial hypercellularity scores. $^{**}p = 0.006$. Data for C and D are mean ± SD; n = 5 mice per group.
(E) Representative Western blot of kidney lysates from vehicle- or XMU-MP-1-treated Het mice, probed for p-MST1, p-YAP, cleaved caspase-3, and GAPDH.
(F) Quantification of protein levels from (E), normalized to GAPDH. Data are mean ± SD; $n = 5$ mice per group; $^{*}p < 0.05$, $^{**}p < 0.01$ vs., Het+Vehicle.

mice showed significantly reduced expression of p-MST1, p-YAP, and cleaved Caspase-3 proteins ($p < 0.01$; $n = 5$ per group; Figures 5E,F). These results suggest that XMU-MP-1 reduces podocyte apoptosis in FAM40A+/- mice by inhibiting the activation of the MST1/2-YAP axis.

## Discussion

This study establishes a critical role for FAM40A as an upstream regulator of the Hippo pathway in the pathogenesis of FSGS. Utilizing a heterozygous FAM40A knockout mouse model for the first time, we demonstrate that partial loss of FAM40A relieves inhibition of MST1/2

kinases, leading to Hippo pathway activation and triggering YAP-dependent podocyte apoptosis. Furthermore, we confirmed that FAM40A deficiency elicits key FSGS clinical phenotypes -- including proteinuria, renal dysfunction, glomerulosclerosis, and mesangial hyperplasia -- mechanistically linked to the induction of podocyte apoptosis and effacement of foot processes (Figure 6). Our intervention with XMU-MP-1, a selective MST1/2 inhibitor, partially rescued these phenotypes, providing proof-of-concept for targeting this axis. However, it is important to note that this was a short-term intervention study in mice. The long-term efficacy, safety, and translational feasibility of MST1/2 inhibition, as well as potential systemic consequences of modulating this fundamental pathway, require thorough future investigation. Collectively, these findings reveal the essential contribution of FAM40A to FSGS development, specifically through its novel regulatory mechanism involving Hippo pathway-mediated podocyte apoptosis, thereby highlighting the FAM40A-MST1/2-YAP axis as a promising therapeutic target for FSGS.

The Hippo signaling cascade is an

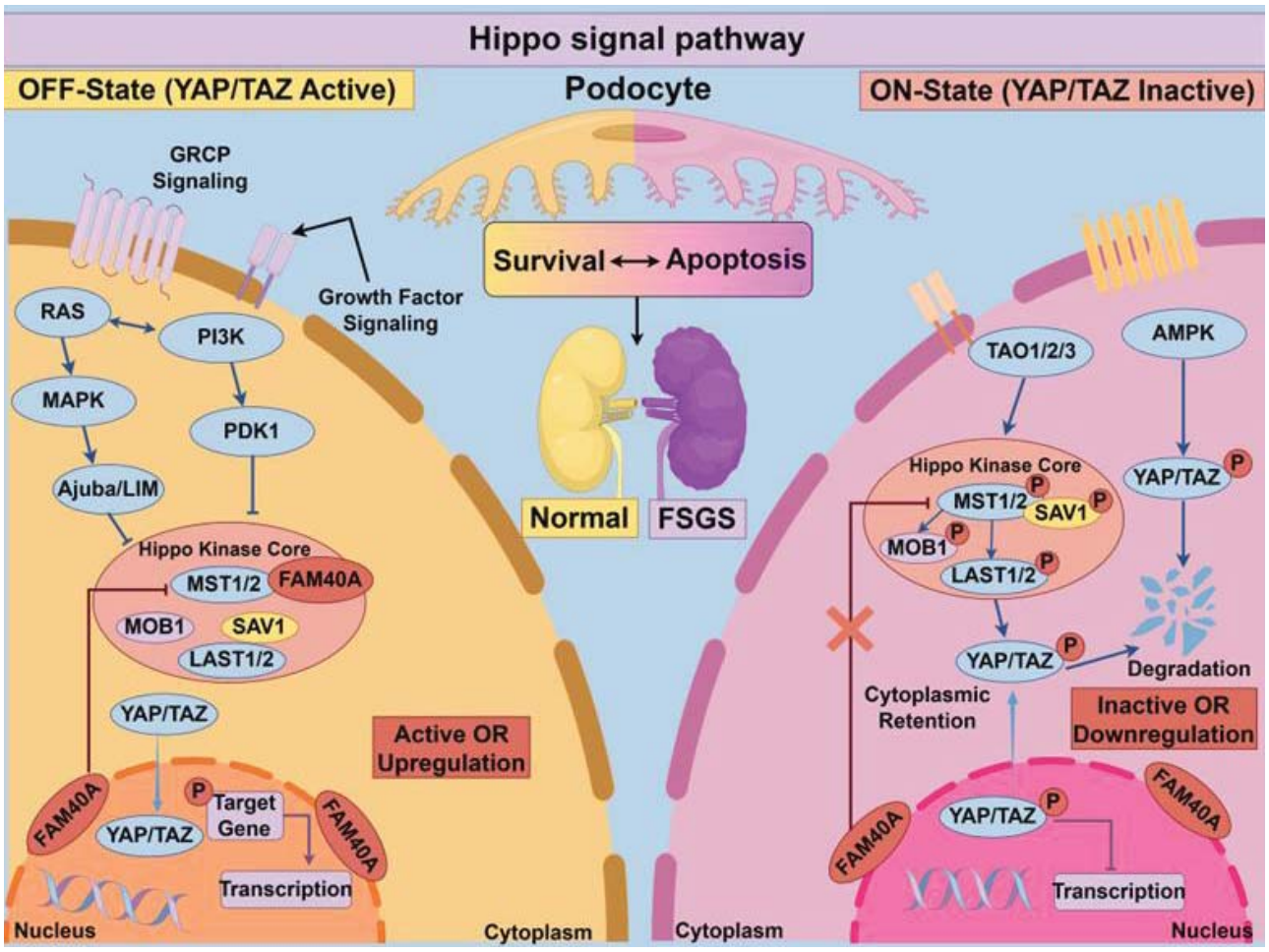


**Figure 6** Schematic model of the proposed FAM40A-MST1/2-YAP axis in FSGS pathogenesis. In healthy podocytes (Left), FAM40A binds to and inhibits MST1/2 kinase activity, keeping the Hippo pathway "OFF." This allows dephosphorylated YAP to translocate to the nucleus, where it promotes pro-survival gene expression, maintaining podocyte integrity.In FAM40A deficiency (Right), the inhibitory effect on MST1/2 is relieved. Activated MST1/2 phosphorylates LATS1/2, which in turn phosphorylates YAP. Phosphorylated YAP (P-YAP) is retained in the cytoplasm and degraded, leading to loss of its nuclear pro-survival signals. This Hippo pathway activation cascade promotes podocyte apoptosis, foot process effacement, and ultimately contributes to the development of FSGS.

evolutionarily conserved serine/threonine kinase network that governs organ size, tissue homeostasis and tumorigenesis through a kinase-to-transcriptional-co-activator relay. At its core lie the MST1/2 and their effector kinases LATS1/2, together with the downstream transcriptional co-activators YAP and TAZ. The pathway oscillates between two functional states. In the "ON" state, elevated cell density or loss of polarity engages MST1/2, assisted by the scaffold SAV1, to phosphorylate LATS1/2 at both the activation loop and hydrophobic motif; the LATS1/2–MOB1 complex then tags YAP/TAZ on Ser127/Ser89. Phosphorylated YAP/TAZ is sequestered in the cytoplasm by 14-3-3 proteins and subsequently degraded *via* a-TrCP-mediated ubiquitin–proteasome route. Persistent activation of this cascade ultimately tips the balance toward apoptosis. Conversely, in the "OFF" state, extracellular cues such as growth factors or mechanical stretch restrain MST1/2 or LATS1/2 activity, thereby preventing YAP/TAZ phosphorylation. Hypo-phosphorylated YAP/TAZ rapidly translocate to the nucleus, partner with TEAD transcription factors and up-regulate pro-survival and anti-apoptotic genes including CTGF, CYR61, AXL and BCL2L1. By coupling reversible phosphorylation to sub-cellular trafficking, the MST1/2–LATS1/2–YAP/TAZ axis integrates diverse environmental inputs to dictate cell fate, and its dysregulation has been implicated in an expanding spectrum of renal and extra-renal pathologies [15,18].

In recent years, research has shown that the role of the Hippo pathway in kidney disease is increasingly recognized, especially its importance in podocyte-related diseases such as FSGS. YAP, a key downstream effector of Hippo signaling, activates multiple nuclear transcription factors to regulate cellular proliferation and apoptosis. In renal podocytes, YAP predominantly localizes to the nucleus, co-localizing with the podocyte-specific nuclear marker WT1. Critically, YAP nuclear activity is indispensable for podocyte survival both *In vivo* and *In vitro*; targeted deletion of YAP in cultured podocytes results in rapid cell death [19]. Supporting this paradigm, Zhuang et al. [16] demonstrated that nuclear localization and activation of YAP constitute an essential endogenous anti-apoptotic mechanism during FSGS progression. Conversely, experimental activation of the Hippo pathway upstream cascade proves detrimental: Wennmann DO, et al. [20] reported that overexpressing WWC1/KIBRA, an activator of the Hippo kinase LATS, induces apoptosis in podocytes *In vitro*. This finding is corroborated *In vivo* by Schwartzman M, et al. [21], who observed that podocyte-specific YAP deletion triggers podocyte apoptosis, proteinuria, and FSGS lesions in mice. Clinical evidence further implicates Hippo pathway dysregulation in human FSGS. Meliambro K, et al. [22] identified increased phosphorylation of YAP (p-YAP, indicative of YAP inactivation) in podocytes of FSGS patients, correlating with disease severity. Their work, alongside emerging studies, suggests that sustained activation of the Hippo pathway within podocytes represents a fundamental mechanism driving glomerulosclerosis and progressive renal function loss [16,23].

In our experiments, podocytes from FAM40A+/- heterozygous mice exhibited cytoplasmic accumulation of p-YAP, indicating YAP inactivation and impaired nuclear translocation necessary for its transcriptional activity. The concurrent elevation of p-MST1 (a key pathway initiator) and p-YAP signifies sustained activation of the Hippo pathway. Consequently, the loss of the Hippo pathway's anti-apoptotic function triggered Caspase-3 activation, culminating in podocyte apoptosis and the development of FSGS. This observed nuclear exclusion of YAP aligns with findings by Zhuang Q, et al. [24]. Furthermore, in adriamycin (doxorubicin)-induced FSGS models, YAP nuclear exclusion exacerbated podocyte

apoptosis and disease progression. Critically, treatment of these models with verteporfin, a YAP inhibitor, induced YAP nuclear exclusion, thereby accelerating podocyte apoptosis and worsening disease outcomes. Their study demonstrated a positive correlation between increased podocyte apoptosis and cytoplasmic YAP localization in human FSGS. In addition to inducing apoptosis, new research has demonstrated that YAP also plays an important role in podocyte adhesion. In YAP knockout mouse models, reduced levels of α3β1 integrin and podocyte adhesion were observed, leading to segmental or global glomerulosclerosis and a significant increase in proteinuria. Mechanistically, this is achieved by YAP through transcriptional regulation of α3β1 integrin *via* TEAD3 [25,26].

The Hippo signaling pathway represents a crucial regulator of fundamental cellular processes, including proliferation, apoptosis, migration, and tissue development and regeneration. Within the kidney, dysregulation of the Hippo pathway is increasingly recognized as a core mechanism underpinning the pathogenesis of FSGS [16,27]. Our findings substantiate this paradigm by demonstrating that FAM40A acts as a critical upstream modulator, negatively regulating MST1/2 kinase activity to prevent hyperactivation of the Hippo pathway. Specifically, loss of FAM40A function derepresses MST1/2 kinase activity. This deregulation promotes phosphorylation-dependent inactivation of the downstream effector YAP, ultimately triggering podocyte apoptosis and culminating in the development of FSGS. Our study confirms that FAM40A deficiency can cause FSGS. We also propose for the first time that the FAM40A-MST1/2-YAP signaling axis plays a key role in podocyte damage, providing a new theoretical framework for targeted intervention and treatment of FSGS. The involvement of FAM40A/STRIP1 within the larger STRIPAK complex suggests that other components of this complex may also be relevant to FSGS pathogenesis, opening new avenues for genetic and mechanistic exploration.

## Conclusion

Our study demonstrated that FAM40A deficiency induces podocyte apoptosis by inactivating YAP through relieving the inhibition of the core Hippo pathway kinases MST1/2. Short-term pharmacological inhibition of MST1/2 ameliorated disease features, thereby providing proof-of-concept for targeting this axis. However, further investigations were required to evaluate the long-term effects and translational potential of modulating the Hippo pathway in renal disease (Supplementary Tables 1-3)**Declaration**

### Ethics approval and consent to participate

All animal experiments were approved by the Institutional Animal Care and Use Committee of Naval Medical University All procedures were conducted in accordance with relevant guidelines and regulations.

### Consent for publication

Not applicable.

### Availability of data and materials

The data that support the findings of this study are available from the corresponding author upon reasonable request.

### Competing interests

The authors declare that they have no competing interests.

### Funding

This study was supported by the Naval Medical University General Incubation Fund (No: 2022MS027).

### Authors contributions

ZC: Conceptualization, Investigation, Formal analysis, Data Curation, Writing – Original

Draft. ZG: Conceptualization, Methodology, Resources, Supervision, Writing – Review & Editing, Funding acquisition. All authors read and approved the final manuscript.

## Acknowledgements

Not applicable.

## References

1. Altintas MM, Agarwal S, Sudhini Y, Zhu K, Wei C, Reiser J. Pathogenesis of Focal Segmental Glomerulosclerosis and Related Disorders. Annu Rev Pathol. 2025 Jan;20(1):329-353. doi: 10.1146/annurev-pathol-051220-092001. PMID: 39854184; PMCID: PMC11875227.
2. Suresh V, Stillman IE, Campbell KN, Meliambro K. Focal Segmental Glomerulosclerosis. Adv Kidney Dis Health. 2024 Jul;31(4):275-289. doi: 10.1053/j.akdh.2024.03.009. PMID: 39084753.
3. Rosenberg AZ, Kopp JB. Focal Segmental Glomerulosclerosis. Clin J Am Soc Nephrol. 2017 Mar 7;12(3):502-517. doi: 10.2215/CJN.05960616. Epub 2017 Feb 27. Erratum in: Clin J Am Soc Nephrol. 2018 Dec 7;13(12):1889. doi: 10.2215/CJN.12071018. PMID: 28242845; PMCID: PMC5338705.
4. Sadowski CE, Lovric S, Ashraf S, Pabst WL, Gee HY, Kohl S, Engelmann S, Vega-Warner V, Fang H, Halbritter J, Somers MJ, Tan W, Shril S, Fessi I, Lifton RP, Bockenhauer D, El-Desoky S, Kari JA, Zenker M, Kemper MJ, Mueller D, Fathy HM, Soliman NA; SRNS Study Group; Hildebrandt F. A single-gene cause in 29.5% of cases of steroid-resistant nephrotic syndrome. J Am Soc Nephrol. 2015 Jun;26(6):1279-89. doi: 10.1681/ASN.2014050489. Epub 2014 Oct 27. PMID: 25349199; PMCID: PMC4446877.
5. Chen Z, Zhang Y, Zhao X. FAM40A alters the cytoskeleton of podocytes in familial focal and segmental glomerulosclerosis by regulating F-actin and nephrin. Arch Med Sci. 2019 Jan;15(1):165-173. doi: 10.5114/aoms.2018.73138. Epub 2018 Feb 2. PMID: 30697267; PMCID: PMC6348344.
6. Madsen CD, Hooper S, Tozluoglu M, Bruckbauer A, Fletcher G, Erler JT, Bates PA, Thompson B, Sahai E. STRIPAK components determine mode of cancer cell migration and metastasis. Nat Cell Biol. 2015 Jan;17(1):68-80. doi: 10.1038/ncb3083. Epub 2014 Dec 22. PMID: 25531779; PMCID: PMC5354264.
7. Bai SW, Herrera-Abreu MT, Rohn JL, Racine V, Tajadura V, Suryavanshi N, Bechtel S, Wiemann S, Baum B, Ridley AJ. Identification and characterization of a set of conserved and new regulators of cytoskeletal organization, cell morphology and migration. BMC Biol. 2011 Aug 11;9:54. doi: 10.1186/1741-7007-9-54. Erratum in: BMC Biol. 2024 Oct 10;22(1):228. doi: 10.1186/s12915-024-02036-3. PMID: 21834987; PMCID: PMC3201212.
8. Tang Y, Chen M, Zhou L, Ma J, Li Y, Zhang H, Shi Z, Xu Q, Zhang X, Gao Z, Zhao Y, Cheng Y, Jiao S, Zhou Z. Architecture, substructures, and dynamic assembly of STRIPAK complexes in Hippo signaling. Cell Discov. 2019 Jan 8;5:3. doi: 10.1038/s41421-018-0077-3. PMID: 30622739; PMCID: PMC6323126.
9. Hwang J, Pallas DC. STRIPAK complexes: structure, biological function, and involvement in human diseases. Int J Biochem Cell Biol. 2014 Feb;47:118-48. doi: 10.1016/j.biocel.2013.11.021. Epub 2013 Dec 11. PMID: 24333164; PMCID: PMC3927685.
10. Chen R, Xie R, Meng Z, Ma S, Guan KL. STRIPAK integrates upstream signals to initiate the Hippo kinase cascade. Nat Cell Biol. 2019 Dec;21(12):1565-1577. doi: 10.1038/s41556-019-0426-y. Epub 2019 Dec 2. Erratum in: Nat Cell Biol. 2020 Feb;22(2):257. doi: 10.1038/s41556-019-0460-9. PMID: 31792377.
11. Zhuang Q, Li F, Liu J, Wang H, Tian Y, Zhang Z, Wang F, Zhao Z, Chen J, Wu H. Nuclear exclusion of YAP exacerbates podocyte apoptosis and disease progression in Adriamycin-induced focal segmental glomerulosclerosis. Lab Invest. 2021 Feb;101(2):258-270. doi: 10.1038/s41374-020-

00503-3. Epub 2020 Nov 17. PMID: 33203894; PMCID: PMC7815513.

12. Gilhaus K, Cepok C, Kamm D, Surmann B, Nedvetsky PI, Emich J, Sundukova A, Saatkamp K, Nüsse H, Klingauf J, Wennmann DO, George B, Krahn MP, Pavenstädt HJ, Vollenbröker BA. Activation of Hippo Pathway Damages Slit Diaphragm by Deprivation of Ajuba Proteins. J Am Soc Nephrol. 2023 Jun 1;34(6):1039-1055. doi: 10.1681/ASN.0000000000000107. Epub 2023 Mar 16. PMID: 36930055; PMCID: PMC10278832.

13. Ester L, Cabrita I, Ventzke M, Kieckhöfer E, Christodoulou M, Mandel AM, Diefenhardt P, Fabretti F, Benzing T, Habbig S, Schermer B. The role of the FSGS disease gene product and nuclear pore protein NUP205 in regulating nuclear localization and activity of transcriptional regulators YAP and TAZ. Hum Mol Genet. 2023 Nov 3;32(22):3153-3165. doi: 10.1093/hmg/ddad135. PMID: 37565816; PMCID: PMC10630254.

14. Zhang N, Shen X, Yu Y, Xu L, Wang Z, Zhu J. Lead exposure promotes NF2-wildtype meningioma cell proliferation through the Merlin-Hippo signaling pathway. Environ Health Prev Med. 2025;30:8. doi: 10.1265/ehpm.24-00216. PMID: 39894505; PMCID: PMC11790403.

15. Ma S, Meng Z, Chen R, Guan KL. The Hippo Pathway: Biology and Pathophysiology. Annu Rev Biochem. 2019 Jun 20;88:577-604. doi: 10.1146/annurev-biochem-013118-111829. Epub 2019 Dec 19. PMID: 30566373.

16. Erekat NS. Apoptosis and its role in renal diseases. In cell death - aAutophagy, apoptosis and necrosis. Intechopen.

17. Bazzi H, Soroka E, Alcorn HL, Anderson KV. STRIP1, a core component of STRIPAK complexes, is essential for normal mesoderm migration in the mouse embryo. Proc Natl Acad Sci U S A. 2017 Dec 19;114(51):E10928-E10936. doi: 10.1073/pnas.1713535114. Epub 2017 Dec 4. PMID: 29203676; PMCID: PMC5754794.

18. Moya IM, Halder G. Hippo-YAP/TAZ signalling in organ regeneration and regenerative medicine. Nat Rev Mol Cell Biol. 2019 Apr;20(4):211-226. doi: 10.1038/s41580-018-0086-y. PMID: 30546055.

19. Bonse J, Wennmann DO, Kremerskothen J, Weide T, Michgehl U, Pavenstädt H, Vollenbröker B. Nuclear YAP localization as a key regulator of podocyte function. Cell Death Dis. 2018 Aug 28;9(9):850. doi: 10.1038/s41419-018-0878-1. PMID: 30154411; PMCID: PMC6113334.

20. Wennmann DO, Vollenbröker B, Eckart AK, Bonse J, Erdmann F, Wolters DA, Schenk LK, Schulze U, Kremerskothen J, Weide T, Pavenstädt H. The Hippo pathway is controlled by Angiotensin II signaling and its reactivation induces apoptosis in podocytes. Cell Death Dis. 2014 Nov 13;5(11):e1519. doi: 10.1038/cddis.2014.476. PMID: 25393475; PMCID: PMC4260734.

21. Schwartzman M, Reginensi A, Wong JS, Basgen JM, Meliambro K, Nicholas SB, D'Agati V, McNeill H, Campbell KN. Podocyte-Specific Deletion of Yes-Associated Protein Causes FSGS and Progressive Renal Failure. J Am Soc Nephrol. 2016 Jan;27(1):216-26. doi: 10.1681/ASN.2014090916. Epub 2015 May 26. PMID: 26015453; PMCID: PMC4696566.

22. Meliambro K, Wong JS, Ray J, Calizo RC, Towne S, Cole B, El Salem F, Gordon RE, Kaufman L, He JC, Azeloglu EU, Campbell KN. The Hippo pathway regulator KIBRA promotes podocyte injury by inhibiting YAP signaling and disrupting actin cytoskeletal dynamics. J Biol Chem. 2017 Dec 22;292(51):21137-21148. doi: 10.1074/jbc.M117.819029. Epub 2017 Oct 5. PMID: 28982981; PMCID: PMC5743086.

23. Fu J, Guan KL. The hippo signalling pathway and its implications in kidney homeostasis and disease. Nature reviews. Nephrology.2023;19(10):672-684.

24. Zhuang Q, Li F, Liu J, Wang H, Tian Y, Zhang Z, Wang F, Zhao Z, Chen J, Wu H. Nuclear exclusion of YAP exacerbates podocyte apoptosis and disease progression in Adriamycin-induced focal segmental glomerulosclerosis. Lab Invest. 2021 Feb;101(2):258-270. doi: 10.1038/s41374-020-00503-3. Epub 2020 Nov 17. PMID: 33203894;

PMCID: PMC7815513.

25. Shao G, Xu J, Hu C, Jia W, Xu X, Gu Y, Zhang L, Zheng Z, Zhong J, Zhu S, Meng S, Zhao Z, Zhang Z, Liu J, Xu Y, Wu H. Podocyte YAP ablation decreases podocyte adhesion and exacerbates FSGS progression through α3β1 integrin. J Pathol. 2025 Jan;265(1):84-98. doi: 10.1002/path.6370. PMID: 39668547.

26. Kato K, Maehama T. The role of YAP/TAZ in integrin-mediated mechanotransduction. Journal of cell science. 2024;137(5): 261545.

27. Vollenbröker B, George B, Wolfgart M, Saleem M A, Pavenstädt H, Weide T. The Hippo pathway in kidney diseases. Cellular signalling. 2019;65:109420.